Physics and chemistry of photocatalytic titanium dioxide: Visualization of bactericidal activity using atomic force microscopy

S. Banerjee[1,3,*], Judy Gopal[2], P. Muraleedharan[2], A. K. Tyagi[1] and Baldev Raj[1]

[1]Materials Science Division and
[2]Corrosion Science and Technology Division,
Indira Gandhi Centre for Atomic Research, Kalpakkam 603 102, India
[3]On deputation from Surface Physics Division, Saha Insitute of
Nuclear Physics, 1/AF Bidhannagar, Kolkata 700 064, India

When titanium dioxide (TiO_2) is exposed to near-ultraviolet light, it exhibits strong bactericidal activity. Anatase phase of TiO_2 film was prepared by anodizing pure titanium coupons (substrate). Atomic force microscopy (AFM) technique was used to image the transformation of titanium surface to TiO_2 surface on anodization. We observed wide distribution of TiO_2 particles ranging from submicron to nanometre sizes, fully covering the substrate forming a thin film on anodizing. With the formation of a thin film of TiO_2, we observed strong bactericidal activity. Bactericidal activity was attributed to the well-known photocatalytic property of the semiconductor TiO_2. Here we present some arguments for reasoning out why certain semiconducting metal oxides exhibit photocatalytic properties and some do not. We also present some of the important elementary reaction steps considering adsorbed oxygen and water molecule as necessary molecules for the photooxidation process. Other reactions involved in producing reactive oxygen species and hydroxyl radical are presented to understand the process involved in photocatalytic biocidal activity. Finally, we present visualization of photocatalytic bactericidal activity of TiO_2 using AFM.

Keywords: Atomic force microscopy, bactericidal activity, photocatalytic effect, titanium dioxide.

IT is now well known that titanium dioxide (TiO_2) is one of the most superior material for decomposing organic materials due to its strong photocatalytic property. It has become the most important photocatalyst in environmental bio-decontamination for a large variety of organics, bacteria, viruses, fungi and cancer cells, which can be totally degenerated and converted to CO_2, H_2O and harmless inorganic anions[1]. The photocatalytic and hence the biocidal activity can be significantly enhanced by reducing the size of the TiO_2 particle[2–4]. By reducing the size of the TiO_2 particle, the surface area of TiO_2 increases leading to improvement of photoefficiency and thus photocatalytic property, because high surface area would make the surface of the particle more active to light and H_2O adsorption. We have

*For correspondence. (e-mail: sangambanerjee@hotmail.com)

prepared a thin film of TiO_2 comprising of sub-micron and clusters of nanoparticle by anodizing pure titanium coupons (substrate). We present here first the photocatalytic process and the reaction chain involved in biocidal activity illustratively. We also present a systematic investigation of the structure and morphology of the bacteria and TiO_2 film using atomic force microscopy (AFM).

The photocatalytic biocidal effect of TiO_2 was first reported by Matsunaga and coworkers[5]. They observed that when TiO_2–Pt catalyst in contact with the microbial cell is exposed to near-ultraviolet light, the microbial cells in water could be killed. The killing/biocidal mechanism(s) by the photocatalytic reaction is still not well understood. However, we will try to present concisely, the physical and chemical processes occurring during the photocatalysis process of TiO_2, which causes biocidal activity in the presence of oxygen and water molecule. By invoking the electronic energy band structure of TiO_2, one can describe its photocatalytic activity. TiO_2 is a large band-gap semiconductor. The outermost filled orbitals of elemental titanium (Ti) are $4s^2$ and $3d^2$ and that of oxygen (O) are $2s^2$ and $2p^4$. In TiO_2, the Ti ions are in a distorted octahedral environment and formally have a $Ti^{4+}(3d^0)$ electronic configuration. The valence band of TiO_2 is composed primarily of oxygen 2p orbitals hybridized with Ti 3d states, while the conduction band is made up of pure 3d orbital of titanium[6–8]. When TiO_2 is exposed to near-UV light, electrons in the valence band are excited to the conduction band leaving behind holes, as shown schematically in Figure 1. The excited electrons in the conduction band are now in a pure 3d state and since the nature of valence and conduction band is completely different, i.e. dissimilar parity, the transition probability of e^- to the valence band reduces leading to reduction of e^-–h^+ recombination. Whereas for the other 3d-transition metal oxide members in the series, 3d-states are present in both the valence band as well as in conduction band. The photoexcited e^-–h^+ pair has similar parity (orbital nature) and hence can recombine faster. The last member of the 3d-transition metal oxide series is ZnO, with Zn having completely filled 3d orbitals ($3d^{10}$). The valence band of ZnO consists of only d-states and the conduction band consists of s–p hybridized orbitals. Thus, the photoexcited e^-–h^+ pair has dissimilar parity like TiO_2 and hence it also will exhibit low recombination probability. Thus, TiO_2 and ZnO are the only two among the 3d-transition metal oxide semiconductor series which remain stable on photoexcitation[9–11]. Whereas for most of the transition metal oxide semiconductors the photoexcited state is generally unstable, leading to recombination of the photogenerated e^-–h^+ pair and thus resulting into heat. This band picture assures a sufficiently long lifetime of e^-–h^+ pair to diffuse to the surface of the catalyst and initiate a redox reaction. Here, we will not deal with the photocatalytic activity of ZnO, but similar arguments can be applied for understanding its photocatalytic property.
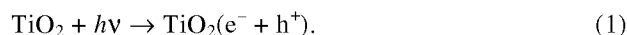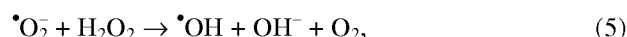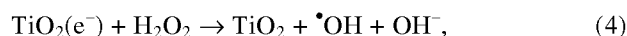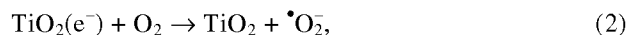
Reduction of A   **Oxidation of D**
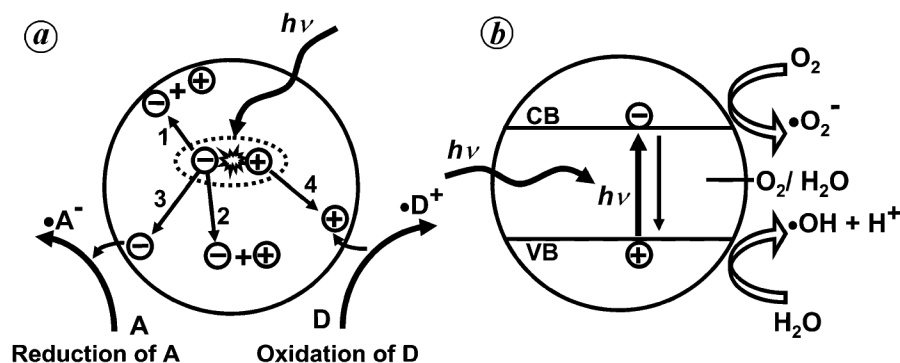
Figure 1. Schematic representation of some of the main processes occurring on a semiconductor particle. *a*, Absorbtion of photon and electron–hole pair formation and migration of electron and hole: arrows marked (1) and (2) show electron–hole recombination at surface and bulk respectively, and those marked (3) reduction of acceptor and (4) oxidation of donor. *b*, On absorbtion of photon of energy $h\nu$, electrons are excited from valence band (VB) to conduction band (CB). There is transfer of electron to oxygen molecule to form superoxide ion radical ($^{\bullet}O_2^-$) and transfer of electron from water molecule to VB hole to form hydroxyl radical ($^{\bullet}OH$).

There are three types of crystal structure in TiO_2: (1) anatase, (2) rutile and (3) brookite type. The band gap value[12] for the anatase type is 3.2 eV, for the rutile type is 3.02 eV and for the brookite type 2.96 eV. Thus, light of wavelength $\lambda < 385$ nm, will excite e^- from the valence band to the conduction band, producing an e^-–h^+ pair. A photocatalyst is characterized by its ability to adsorb simultaneously two reactants, which can be reduced and oxidized by efficiently absorbing light ($h\nu \geq E_g$). And, also on the ability to transfer electron from the conduction band to the adsorbed particle (acceptor), which is governed by the band energy position of the semiconductor and the redox potentials of the adsorbate. From the thermodynamic point of view, the redox potential of the adsorbate (acceptor) should be below the conduction band of the semiconductor. If the adsorbate is the donor, then the potential level of the adsorbate (donor) should be above the valence band position of the semiconductor in order to donate an electron to the empty hole in the valence band. The process of transfer of electron from the semiconductor to the adsorbate is called the reduction mechanism and the process of transfer of electron from the adsorbate to the semiconductor is called the oxidation mechanism. These processes are described illustratively in Figure 1. Thus, the energy level at the bottom of conduction band determines the reduction ability of photoelectrons and the energy level at the top of valence band determines the oxidizing ability of photoholes. If the adsorbed couples are considered to be water and dissolved oxygen (H_2O/O_2), then water gets oxidized by positive holes and it splits into $^{\bullet}OH$ and H^+. Since oxygen is an easily reducible substance, reduction of oxygen by the photoelectron of the conduction band results in generation of superoxide radical anions ($^{\bullet}O_2^-$), which in turn reacts with H^+ to generate hydrogen dioxide radical ($^{\bullet}HO_2$, hydroperoxyl). On subsequent collisions with an electron to produce a hydrogendioxide(1–) anion (HO_2^-, hydrogenperoxide(1–)), and then with hydrogen
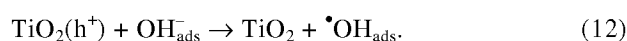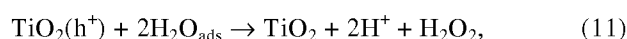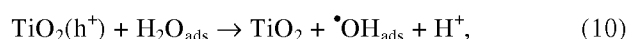
ion, a molecule of H_2O_2 is eventually produced. The above chain of reactions and other reactions involved in producing reactive oxygen species (ROS) such as H_2O_2, $^{\bullet}O_2^-$, etc. and hydroxyl radical $^{\bullet}OH$ are described below: The photocatalytic process begins with absorbtion of photon ($h\nu$):

$$TiO_2 + h\nu \rightarrow TiO_2(e^- + h^+). \tag{1}$$

Reactions involving conduction band e^-

$$TiO_2(e^-) + O_2 \rightarrow TiO_2 + {}^{\bullet}O_2^-, \tag{2}$$

$$TiO_2(e^-) + {}^{\bullet}O_2^- + 2H^+ \rightarrow TiO_2 + H_2O_2, \tag{3}$$

$$TiO_2(e^-) + H_2O_2 \rightarrow TiO_2 + {}^{\bullet}OH + OH^-, \tag{4}$$

$${}^{\bullet}O_2^- + H_2O_2 \rightarrow {}^{\bullet}OH + OH^- + O_2, \tag{5}$$

$${}^{\bullet}O_2^- + H^+ \rightarrow {}^{\bullet}HO_2, \tag{6}$$

$$TiO_2(e^-) + {}^{\bullet}HO_2 \rightarrow TiO_2 + HO_2^-, \tag{7}$$

$$HO_2^- + H^+ \rightarrow H_2O_2, \tag{8}$$

$$2\,{}^{\bullet}HO_2 \rightarrow O_2 + H_2O_2. \tag{9}$$

Reactions involving valence band h^+

$$TiO_2(h^+) + H_2O_{ads} \rightarrow TiO_2 + {}^{\bullet}OH_{ads} + H^+, \tag{10}$$

$$TiO_2(h^+) + 2H_2O_{ads} \rightarrow TiO_2 + 2H^+ + H_2O_2, \tag{11}$$

$$TiO_2(h^+) + OH^-_{ads} \rightarrow TiO_2 + {}^{\bullet}OH_{ads}. \tag{12}$$
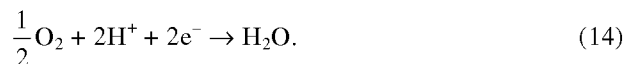
ROS and hydroxyl radicals cause damage to various cell components leading to biocidal activity induced by photo-

catalysis. Subsequently, termination reactions also take place during the above process:

$$^{\bullet}OH + H^+ + 2e^- \rightarrow H_2O, \tag{13}$$

$$\frac{1}{2}O_2 + 2H^+ + 2e^- \rightarrow H_2O. \tag{14}$$

The hydroxyl-free radical $^{\bullet}OH$ is highly reactive, short-lived and detrimental. It can penetrate cell walls and break DNA strands. Superoxide anion $^{\bullet}O_2^-$ is more long-lived and cannot penetrate the cell walls due to its negative charge whereas hydrogen peroxide (H_2O_2) can penetrate the cell walls[1]. Superoxide anion and hydrogen peroxide are both highly reactive to biological macromolecules and also act precursors for the hydroxyl radical ($^{\bullet}OH$). The above chain of reactions is shown illustratively in Figure 2. After penetrating the cell wall, H_2O_2 gets activated by ferrous (Fe^{2+}) ion via the Fenton reaction:

$$Fe^{2+} + H_2O_2 \rightarrow Fe^{3+} + ^{\bullet}OH + OH^-. \tag{15}$$
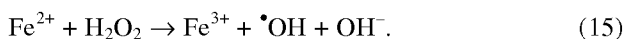
Thus, when TiO_2 is illuminated to produce H_2O_2, the Fenton reaction may take place *in vivo* and produce more hydroxyl radicals. Outside the cell wall, where both H_2O_2 and $^{\bullet}O_2^-$ are present, additional hydroxyl radical $^{\bullet}OH$ is produced via

$$Fe^{3+} + TiO_2(e^-) \rightarrow Fe^{2+}, \tag{16}$$

$$Fe^{3+} + ^{\bullet}O_2^- \rightarrow Fe^{2+} + O_2, \tag{17}$$

and the above Fenton reaction[13,14]. The above-mentioned sequence of chain reactions describe more or less the biocidal activites when TiO_2 is exposed to near-UV radiation in the presence of H_2O and dissolved O_2. Thus, illuminated TiO_2 can decompose and mineralize organic compounds by participating in a series of oxidation reactions leading to carbon dioxide and water.
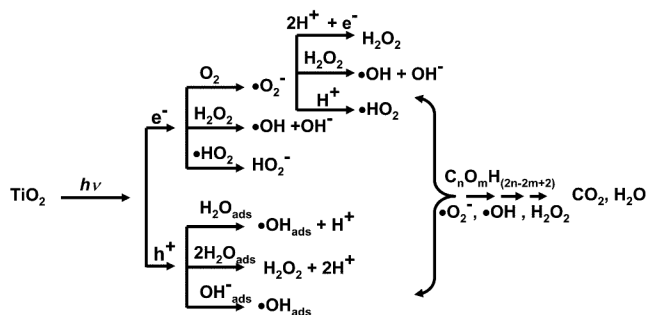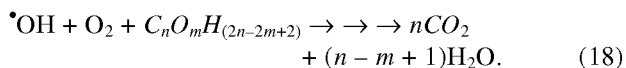
$$^{\bullet}OH + O_2 + C_nO_mH_{(2n-2m+2)} \rightarrow \rightarrow \rightarrow nCO_2 \\ + (n - m + 1)H_2O. \tag{18}$$

Figure 2. Chain of reactions involved in the production of reactive oxygen species such as H_2O_2, $^{\bullet}O_2^-$, etc. and hydroxyl radical $^{\bullet}OH$ shown illustratively.

The above chemical reaction processes can be extended to any organic and bio-microorganisms, including cancer cells.

As mentioned earlier, among the three structures only anatase and rutile are commonly used as photocatalysts. However, it is interesting to note that there exist controversial results regarding the photocatalytic activity among these two phases. But, in general, it is believed that anatase phase[15,16] has greater photocatalytic activity than rutile. There are also studies that the rutile phase has greater photocatalytic activity[17,18] and some studies even claim that a mixture of anatase (70–75)% and rutile (30–25)% is more active than pure anatase[19–21]. The reason is still not understood and more detailed and careful experiments are required to understand this discrepancy. The disagreement of the results may be due to various reasons, such as crystal size, surface area, defects, porosity and pore size distribution. One can reason out that since the anatase phase has a higher Fermi level than the rutile phase by about 0.1 eV, the anatase phase will have lower capacity to adsorb oxygen and higher degree of hydroxylation (i.e. number of hydroxy groups on the surface)[16,22–24] and thus, should have greater photocatalytic activity than the rutile phase. Another essential difference is that the anatase phase has a wider optical absorption gap and may have smaller electron effective mass and hence higher mobility. It has also been reported that the anatase phase has an indirect band gap, whereas the rutile phase has a direct band gap[25,26]. The indirect band gap will cause further decrease in the recombination rate of the e^-–h^+ pair generated upon illumination. Thus, more detailed experimental and theoretical work is required to determine the e^- effective mass and mobility of the photo-generated e^-. It can be argued that higher the mobility of e^-, higher the photocatalytic activity. If the mobility of the photogenerated e^- and h^+ is different, then the recombination probability will also decrease. Ascertaining these will help us in understanding the photocatalytic mechanism further and will give us more clue to design higher and efficient photocatalytic materials. We already have some clues to increase the photocatalytic property. Increasing the e^-–h^+ charge separation will decrease the recombination. This can be achieved by incorporating metals (such as Pt and Ag) and metal oxides (such as RuO_2) on the surface of the TiO_2 particles[15]. The photogenerated e^-s are injected into the metal particle (Pt or Ag) and the h^+s into the metal oxide (RuO2). This increases the e^-–h^+ charge separation and hence reduces the e^-–h^+ recombination, causing increase in efficiency in oxidation and reduction reactions on the particle surfaces. Oxygen vacancy on the surface of the TiO_2 particle will give rise to Ti^{3+}, thus trapping electrons. This also inhibits e^-–h^+ recombination on illumination. It has been also observed that Fe^{3+} and Cu^{2+} doping of TiO_2 inhibits e^-–h^+ recombination[27,28], whereas Cr^{3+} increases the e^-–h^+ recombination[29]. This doping behaviour needs further studies.
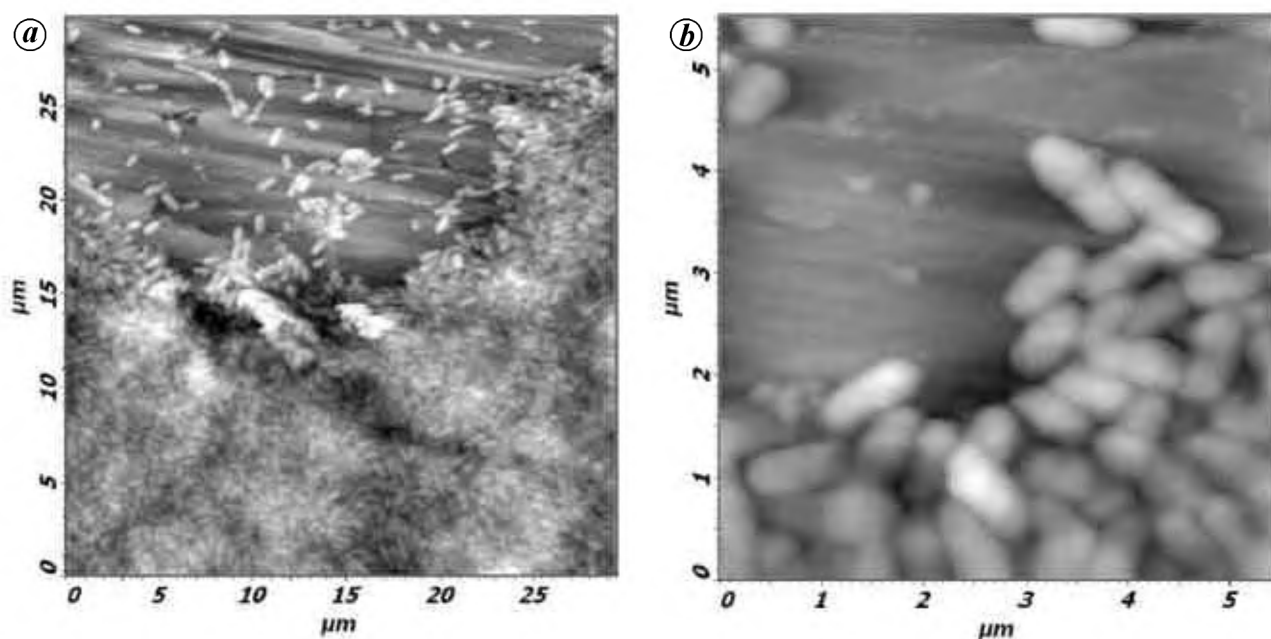
Figure 3. *a*, AFM image of growth of a bacterial colony on unanodized Ti coupon in 30 μm × 30 μm scan area. *b*, At higher magnification (6 μm × 6 μm) we can clearly see the bacteria and the substrate was observed to be smooth.

In the present investigation, a thin film of TiO_2 was prepared by anodizing commercially pure titanium grade-2 coupons (3 cm × 2 cm) in an acid bath (nitric acid 400 g/l + hydrofluoric acid 40 g/l + water) and then ultrasonically cleaned using soap solution to remove all traces of acid from the surface. The coupons were then washed in running water and finally rinsed in distilled water and air-dried. Anodization was carried out at 25°C in orthophosphoric acid (30 g/l) for 48 h at 30 V. It has been observed earlier using grazing incidence X-ray diffraction that on anodization, the phase of TiO_2 is mostly anatase[30]. It is also known that nanoparticles of TiO_2 are generally in anatase phase[31]. Particle size experiments have shown that the relative phase stability may reverse due to surface energy effect, when the particle size decreases[31]. In the nanometer-scale size, the anatase phase may become more stable than the rutile phase, which is otherwise opposite when the particle sizes are bigger. Gram-negative *Pseudomonas* sp. was used as test microorganism to study the bactericidal properties of the anodized coupons. The reason for selection of the above genus is that it has been identified as the major colonizer of freshwater biofilms[32,33]. Both the unanodized and the anodized coupons were placed in a dilute nutrient culture for 100 h. The dilute nutrient culture was prepared by inoculating 1% (0.13 g/l) nutrient broth with 0.1 ml of 24 h culture of *Psuedomonas* sp. in 100% nutrient broth. This culture in dilute nutrient medium was recultured and used for exposure studies. This dilute nutrient culture was used to avoid pelagic growth of bacteria and to favour biofilm formation. The culture was mixed uniformly in an orbital shaker and in-

cubated for 12 h at 32°C before the coupons were introduced. The density of *Psuedomonas* sp. in the exposure medium (500 ml) was 6×10^8 cfu/ml. Exposure studies were conducted in a cylindrical glass vessel containing the dilute nutrient culture. The coupons were placed on a glass rod inside the culture medium. The coupons were illuminated by six numbers of black light blue (BLB) lamps (4W, Philips) arranged in a hexagonal configuration surrounding the cylindrical glass vessel. The light produced by BLB lamps has wavelength range of 350–380 nm and hence is referred to as near-UV light, to distinguish it from the UV light used normally for disinfection. The near-UV light used in the study was found not to have any bactericidal property; it can be transmitted through ordinary glass. AFM was used to visualize the unanodized and anodized surfaces and the attached bacterial cells.

We observed bacterial colony persisting on unanodized coupons even after the coupons were exposed to near-UV light. In Figure 3 *a*, we show the AFM image of growth of a bacterial colony on unanodized Ti coupon in 30 μm × 30 μm scan area. On higher magnification to 6 μm × 6 μm (Figure 3 *b*), we can clearly see the bacteria and the substrate was observed to be smooth. On the anodized coupons, after exposure to near-UV light, we observed almost no bacteria persisting on the coupons. In Figure 4 *a*, we show the AFM image scan on an area of 30 μm × 30 μm of a near-UV exposed anodized coupon. Bacteria are indicated by arrows (we have shown only those selected regions where some bacteria could be seen to compare the texture of the substrate with respect to the structure of bacteria). The bactericidal property of anodized coupons
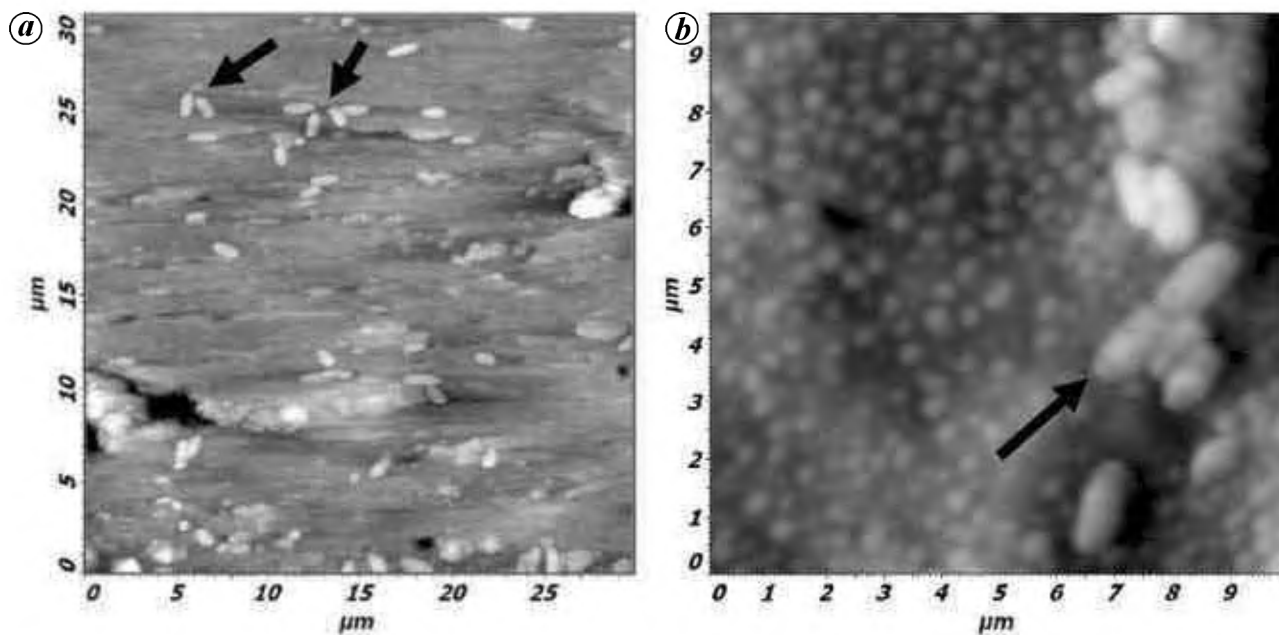
Figure 4. *a*, AFM image scan on an area of 30 μm × 30 μm of a near-UV exposed anodized coupon. Bacteria are indicated by arrows. We observe fully covered small grain-like formation on the surface of Ti coupons on anodization. *b*, Another region (10 μm × 10 μm) showing clear grain formation on Ti coupons upon anodization.
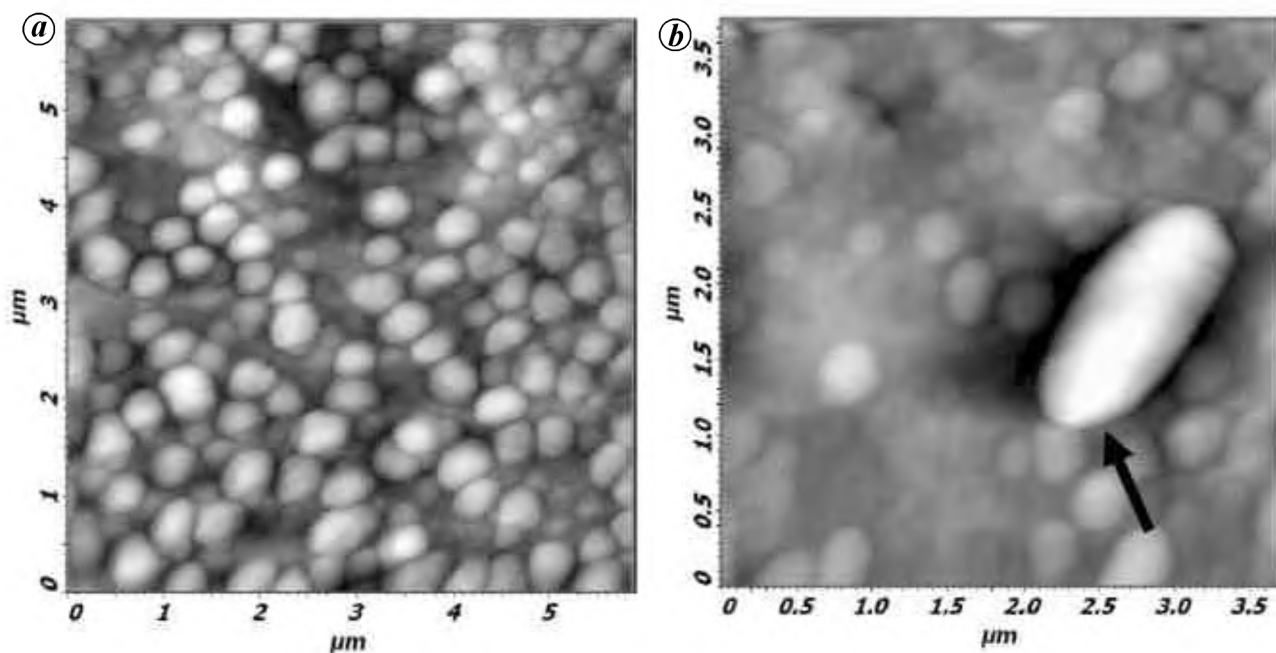

Figure 5. *a*, Magnified region of anodized coupon consisting of grains, the largest size of these grains is ~0.5 μm. *b*, On further magnification we can clearly see smaller grains having sizes down to nanometre scale and bigger grains in clusters of nanometre size (lone bacteria is indicated by an arrow).

using optical method (epifluorescence micrograph) has already been reported earlier[30,34]. This gives large area statistical information about the efficiency of the bactericidal activity of TiO_2 nanoparticles. On magnification to

10 μm × 10 μm area scan (Figure 4 *b*), we observe fully covered, small grain-like formation on the surface of Ti coupons on anodization. In Figure 5 *a*, we show a magnified region consisting of grains and the largest size of these

grains is ~0.5 μm. On further magnification (Figure 5 *b*), we see clearly smaller grains having size down to nanometre scale and bigger grains are in clusters of nanometre size. These grains can be attributed to the formation of submicron and nanometre scale TiO_2 particles on the Ti coupons upon anodization. We are now optimizing the anodization conditions to achieve nano-monodispersed TiO_2 particles and reduce the size further by varying the anodization parameter. Thus, AFM is a powerful tool to visualize the anodization process by imaging the surface morphology. Also, one can see the morphology of the bacteria without special sample preparation. AFM will thus become a powerful tool to visualize the biocidal activities *in situ* and *ex situ*.

To summarize, we have presented in detail some aspects of the photocatalytic process from the physical point of view, by invoking electronic band structure of transition metal semiconducting oxide and argued that if the excited $e^- - h^+$ pair on illumination has dissimilar parity, i.e. the nature of the valence band and the conduction band is different, only then is the $e^- - h^+$ recombination probability reduced. Any oxide showing this type of band structure will show enhanced photocatalytic property. Water and oxygen molecules are considered necessary for the photo-oxidation process. We have also suggested that indirect band gap materials will show better photocatalytic effect than direct band gap materials. This may be one of the reasons why anatase shows higher photocatalytic activity than rutile, apart from having a higher band gap and a higher Fermi level. One has to carry out more systematic studies, theoretically and experimentally, to determine the effective masses of the photogenerated $e^- - h^+$ pairs and their mobility. Unfortunately, to the best of our knowledge, to date there have been no such studies (theoretically as well as experimentally) on this aspect. We have also presented the most common series of elementary chemical reaction steps involved in the generation of ROS, such as H_2O_2, $^\bullet O_2^-$, etc. and hydroxyl radical $^\bullet OH$ responsible for the biocidal activity. We have also visualized biocidal activity using AFM and pointed out the advantage of using this tool. The biocidal activity on anodized coupons was attributed to the formation of submicron and nanometre scale TiO_2 particles and their photocatalytic properties.

1. Blake, D. M., Maness, P., Huang, Z., Wolfrum, E. J. and Huang, J., *Sep. Purif. Methods*, 1999, **28**, 1.
2. Zili, X., Jing, S., Chunming, L., Kang, C., Guo, H. and Du, Y., *Mater. Sci. Eng. B*, 1999, **3**, 211.
3. Qunighong, Z., Lian, G., Jingkun, G., McKinney, B. and Rouse, M., *Appl. Catal. B*, 2000, **26**, 207.
4. Liqiang, J., Xiaojun, S., Weimin, C., Zilli, X., Yaoguo, D. and Honggang, F., *J. Phys. Chem. Solids*, 2003, **64**, 615.
5. Matsunaga, T., Tomodam, R., Nakajima, T. and Wake, H., *FEMS Microbiol. Lett.*, 1985, **29**, 211.
6. Paxton, A. T. and Thien-Nga, L., *Phys. Rev. B*, 1998, **57**, 1579.
7. Khan, M. A., Kotani, A. and Parlebas, J. C., *J. Phys. Condens. Matter*, 1991, **3**, 1763.
8. Halley, J. W. and Shore, H. B., *Phys. Rev. B*, 1987, **36**, 6640.
9. Fortuny, A., Bengoa, C., Font, J. and Fabregat, A., *J. Hazard Mater.*, 1999, **64**, 181.
10. Wissiak, K. S., Sket, B. and Vrtacnik, M., *Chemosphere*, 2000, **41**, 1451.
11. Lui, H. and Yang, T. C., *Process Biochem.*, 2003, **39**, 475.
12. Wunderlich, W., Oekermann, T., Miao, L., Hue, N. T., Tanemura, S. and Tanemura, M., *J. Ceram. Process. Res.*, 2004, **4**, 342.
13. Rupper, G., Bauer, R. and Hesler, G. J., *J. Photochem. Photobiol. A*, 1993, **56**, 113.
14. Safarzadeh-Amiri, A., Bolton, J. R. and Carter, S. R., *J. Adv. Oxid. Technol.*, 1996, **1**, 29.
15. Linsbigler, A. L., Lu, G. Q. and Yates Jr. J. T., *Chem. Rev.*, 1995, **95**, 735.
16. Tanaka, K., Capule, M. F. V. and Hasinaga, T., *Chem. Phys. Lett.*, 1991, **187**, 73.
17. Watson, S. S., Beydoun, D., Scott, J. A. and Amal, R., *Chem. Eng. J.*, 2003, **95**, 213.
18. Mills, A., Lee, S. K. and Lepre, A., *J. Photochem. Photobiol. A: Chem.*, 2003, **155**, 199
19. Basca, R. R. and Kiwi, J., *Appl. Catal. B: Environ*, 1998, **16**, 19.
20. Muggli, D. S. and Ding, L., *Appl. Catal. B: Environ*, 2001, **32**, 181.
21. Ohno, T., Sarukawa, K., Tokeida, K. and Matsumura, M., *J. Catal.*, 2001, **203**, 82.
22. Maruska, H. P. and Ghosh, A. K., *Solar Energy*, 1978, **20**, 443.
23. Gerischer, H. and Heller, A., *J. Electrochem. Soc.*, 1992, **139**, 113.
24. Bickley, R. I., Gonzales-Carreno, T., Lee, J. L., Palmisano, L. and Tilley, R. J. D., *J. Solid State Chem.*, 1991, **92**, 178
25. Mo, S. D. and Ching, W. Y., *Phys. Rev. B*, 1995, **51**, 13023.
26. Reddy, K. M., Manorama, S. V. and Reddy, A. R., *Mater. Chem. Phys.*, 2002, **78**, 239.
27. Butler, E. C. and Davis, A. P., *J. Photochem. Photobiol. A: Chem.*, 1993, **70**, 273.
28. Fujihira, M., Satoh, Y. and Osa, T., *Bull. Chem. Soc. Jpn.*, 1982, **55**, 666.
29. Hermann, J. M., Disdier, J. and Pichat, P., *Chem. Phys. Lett.*, 1984, **108**, 618.
30. Muraleedharan, P., Gopal, J., George, R. P. and Khatak, H. S., *Curr. Sci.*, 2003, **84**, 197.
31. Zhang, H. Z. and Banfield, J. F., *J. Mater. Chem.*, 1998, **8**, 2073; *J. Phys. Chem. B*, 2000, **104**, 3481.
32. George, R. P., Muraleedharan, P., Sreekumari, K. R. and Khatak, H. S., *Biofouling*, 2003, **19**, 1.
33. Rao, T. S., George, R. P., Venugopalan, V. P. and Nair, K. V. K., *Biofouling*, 1997, **11**, 265.
34. Judy Gopal, George, R. P., Muraleedharan, P. and Khatak, H. S., *Biofouling*, 2004, **20**, 167.